

## Research Paper

## Convective heat transfer correlations for Triply Periodic Minimal Surfaces based heat exchangers

Giovanni Brambati<sup>a,\*</sup>, Manfredo Guilizzoni<sup>b</sup>, Stefano Foletti<sup>a</sup><sup>a</sup> Politecnico di Milano, Department of Mechanical Engineering, via La Masa 1, Milan, 20156, Italy<sup>b</sup> Politecnico di Milano, Department of Energy, Via Lambruschini 4, Milan, 20156, Italy

## ARTICLE INFO

## Keywords:

TPMS structures  
Heat exchangers  
Heat transfer correlation  
Computational Fluid Dynamics  
Forced convection

## ABSTRACT

Lattice structures based on Triply Periodic Minimal Surfaces (TPMS) have been extensively studied in the field of heat exchange due to the advantages they can offer in terms of increased heat exchange area and enhanced convective phenomena, thanks to their intricate geometry. Numerous studies have been conducted on fluid motion within these structures, confirming that Computational Fluid Dynamics (CFD) simulations can accurately replicate their thermo-fluid dynamic behavior. However, such simulations are computationally expensive and may be difficult to integrate in larger models of the whole system. Traditionally, heat exchanger design relies on convective heat transfer coefficient correlations based on non-dimensional groups, especially when dealing with turbulent flow. This study proposes a single correlation, based on the results of a series of CFD simulations, to calculate the convective heat transfer coefficient for various fluids and different TPMS topologies and geometries. This is achieved through a careful selection of characteristic lengths for the various non-dimensional groups considered. Within an acceptance range of  $\pm 20\%$ , the predictive capability of the correlation is proved valid for three distinct TPMS topologies: Gyroid, Schwarz-Primitive, and Schwarz-Diamond. It applies across a porosity range of 70% to 90%, considering various unit cell lengths and different fluids. Furthermore, the study presents the effect of viscous heating at high Reynolds numbers on the different topologies and compares the proposed correlation with existing ones.

## 1. Introduction

An effective and efficient exchange of heat is an increasing need in a large number of sectors and applications. To improve heat transfer performances or efficiency, heat exchangers (HX) often incorporate optimized shapes or internal features [1–3]. In recent times, additive manufacturing have demonstrated encouraging outcomes in the production of compact heat exchangers featuring innovative heat transfer designs, due to its capability to create intricate geometries [4,5]. One notable category of materials made feasible by additive manufacturing is architected cellular materials, where a regular lattice structure is repeated throughout the space enhancing their functional properties compared to the bulk material [6]. Architected cellular materials can be divided into two classes: strut-based lattice structures and sheet-based lattice structures. Heat transfer characteristics of strut-based lattice structure have been widely studied in the past few years [7–9] in comparison with open-cell foams [10,11]. In the context of sheet-based lattice structures, the bioinspired [12] Triply Periodic Minimal Surfaces (TPMS) have become the focus of numerous studies [13]. TPMS surfaces are characterized by having a zero-mean curvature,

meaning that the sum of the principal curvatures at each point is zero [14]. The concept of applying TPMS structures to heat exchangers was initially introduced by Slaughter [15], due to the fact that TPMS structures divide a given volume into two separate yet intertwined regions with a smooth and continuous surface.

In recent years, there has been a significant focus on studying fluid flow and heat transfer phenomena within TPMS structures, with both numerical and experimental approaches, and in some of these works heat transfer correlations have been proposed. A significant portion of these studies has concentrated on laminar flow conditions, as evidenced by [16–20]. Among these, studies like those by Kaur et al. [18], Attarzadeh et al. [19], and Iyer et al. [20] were exclusively numerical, while others, such as Femmer et al. [16] and Dixit et al. [17], included both numerical and experimental analyses. Notably, Iyer et al. [20] proposed convective heat transfer coefficient correlations for different topologies, applicable up to a maximum Reynolds number of 350. In the context of turbulent flow conditions, numerical studies by Li et al. [21] compared TPMS structures with printed circuit heat exchangers (PCHE), while Al-Ketan et al. [22] investigated TPMS applications

\* Corresponding author.

E-mail address: [giovanni.brambati@polimi.it](mailto:giovanni.brambati@polimi.it) (G. Brambati).<https://doi.org/10.1016/j.applthermaleng.2024.122492>

Received 27 September 2023; Received in revised form 11 January 2024; Accepted 16 January 2024

Available online 18 January 2024

1359-4311/© 2024 The Author(s). Published by Elsevier Ltd. This is an open access article under the CC BY license (<http://creativecommons.org/licenses/by/4.0/>).

## Nomenclature

### G

$\lambda$	Thermal conductivity (fluid) (W/mK)
$\mu$	Dynamic viscosity (Pa/s)
$\Pi$	Reynolds stress tensor
$\rho$	Density (kg/m <sup>3</sup> )
$\tau$	Stress tensor
$\tau_w$	Wall shear stress (Pa)

### N

$\dot{m}$	Mass-flow rate (kg/s)
$\dot{Q}''$	Heat flux (W/m <sup>2</sup> )
$\dot{Q}$	Heat transfer rate (W)
$\mathbf{w}$	Velocity vector (m/s)
$A_c$	Cross sectional area (m <sup>2</sup> )
$A_{HX}$	Heat exchange surface (m <sup>2</sup> )
$c_p$	Specific heat capacity at constant pressure (J/kg K)
$D$	Diameter (mm)
$D_h$	Hydraulic diameter (mm)
$D_p$	Pore diameter(mm)
$f$	Friction factor
$h$	Convective heat transfer coefficient (W/m <sup>2</sup> K)
$h_{tot}$	Total enthalpy (J/kg)
$L$	General characteristic length (m)
$LMTD$	Logarithmic mean temperature difference (K)
$p$	Pressure (Pa)
$T$	Temperature (K)
$U$	Overall heat transfer coefficient (W/m <sup>2</sup> K)
$V$	Volume of fluid domain (m <sup>3</sup> )
$y^+$	Non-dimensional wall distance
$Nu$	Nusselt number
$Pr$	Prandtl number
$Re$	Reynolds number

### S

$b$	bulk
$c, cold$	cold fluid
$h, hot$	hot fluid
$L, D, D_p, D_h$	Characteristic lengths
$w$	wall

as heat sinks under forced convection. Studies by Khalil et al. [23], Reynolds et al. [24], and Liang et al. [25] stand out for both numerical and experimental analyses, exploring TPMS structures in turbulent flow condition. Noteworthy, correlations for the convective heat transfer coefficient were proposed by Reynolds et al. [24] and Khalil et al. [23], applicable for a maximum Reynolds number of 2500. Additionally, Baobaid [26] investigated natural convection, proposing correlations to estimate the convective heat transfer coefficient with respect to Rayleigh number.

All the conducted studies consistently demonstrated the effectiveness of TPMS lattice structures in the context of heat exchangers and the faithfulness of CFD in replicating fluid flow and heat transfer phenomena. However, in order to facilitate the widespread adoption of heat exchangers with TPMS lattice structures, engineers require tools such as correlations to assist them during the design phase [1,27]. To the author best knowledge, it has not yet been proposed a single

**Table 1**

Thermo-physical properties of the fluids considered.

Fluid	Temperature T [K]	Density $\rho$ [kg/m <sup>3</sup> ]	Specific heat capacity $c$ [J/kg K]	Dynamic viscosity $\mu$ [Pa s]	Thermal conductivity $\lambda$ [W/mK]	Prandtl number $Pr$ [-]
Air	293	–	1006.1	1.82e <sup>-5</sup>	0.0255	0.718
	333	–	1008.1	2.01e <sup>-5</sup>	0.0285	0.710
Water	293	998.2	4184	0.001	0.598	6.997
	333	983.3	4185	4.66e <sup>-4</sup>	0.651	2.995
Acetone	293	790	2160	3.23e <sup>-4</sup>	0.181	3.855
	333	744	2290	2.26e <sup>-4</sup>	0.168	3.081

correlation that is considered valid for different fluids, for different TPMS unit lattices and for different cell dimensions, for the case of high Reynolds numbers ( $Re > 5000$ ). The aim of this study is to use experimentally validated CFD simulations to develop a single correlation for the convective heat transfer coefficient for TPMS in fully turbulent flow condition.

The article is structured as follows: Section 2 describes the numerical model used for the simulations, from the thermo-physical properties of the fluids to the experimental validation of the CFD. Section 3 presents the methodology employed to compute the convective heat transfer coefficient and outline the specific cases used for calibration and validation of the correlation. Afterwards, the results of both calibration and validation are presented in Section 4. The newly proposed correlation will be also compared with two classical and TPMS-specific [24] heat transfer correlations. To keep the use of the proposed correlation the simplest and most customary for researchers, mainly used to low-speed applications, the correlation will be developed using the static temperatures. As the velocities in some of the investigated flow conditions are quite large, an additional version using the total temperatures, which may be more suitable in presence of significant viscous heating, will also be presented in Section 4.3

## 2. Numerical setup

### 2.1. Thermo-physical properties

In this section, the thermo-physical properties of all the fluids considered in this study are presented. During the simulations, no variation of thermo-physical properties have been assumed for each fluid, with different values considered depending on the inlet temperature. The relevant thermo-physical properties of all the fluids are summarized in Table 1. For the case of air, being modeled as a compressible fluid, the density value is not specified explicitly but is computed assuming an ideal fluid behavior.

Concerning the solid domain, this is chosen to be made of aluminum for all the simulations, with a thermal conductivity equal to 181 W/mK [25].

### 2.2. Geometrical domain

In this study, the focus was placed on three TPMS topologies, namely Gyroid, Schwarz-Primitive and Schwarz-Diamond. The choice of these topologies is done in accordance with the study done by [25]. These topologies can be mathematically described using trigonometric functions, with  $x$ ,  $y$  and  $z$  as the Cartesian coordinates. In Fig. 1 the TPMS cells are shown.

$$\sin(x)\cos(y) + \sin(y)\cos(z) + \sin(z)\cos(x) = 0 \quad (1)$$

$$\cos(x) + \cos(y) + \cos(z) = 0 \quad (2)$$

$$\cos(x)\cos(y)\cos(z) - \sin(x)\sin(y)\sin(z) = 0 \quad (3)$$

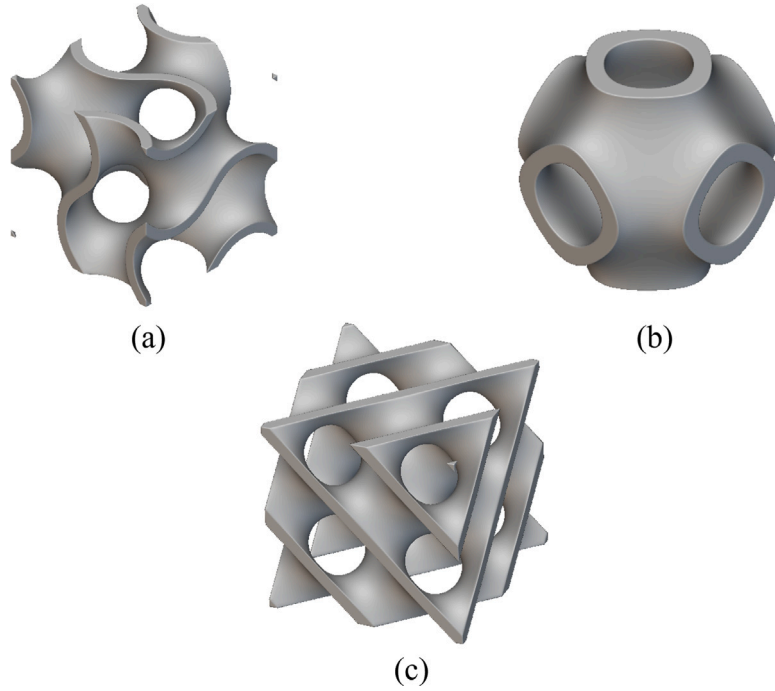


Fig. 1. TPMS cells generated with Ntopology. (a) Gyroid, (b) Schwarz-Primitive, (c) Schwarz-Diamond.

In recent years, various design software tools [28,29] have emerged to facilitate the modeling of TPMS structures. For the purpose of this study, the commercial software Ntopology was chosen in order to obtain the 3D CAD models of the three domains that will be simulated, namely solid domain, hot fluid and cold fluid. To explore the possibility of developing a correlation that is applicable across different geometric dimensions, this study will investigate various unit cell lengths while maintaining a constant porosity value of 81% (defined as the ratio of the void volume in the material to the volume of the associated pure solid unit), by choosing the proper wall thickness value. This choice of porosity value aligns with the porosity value used in the study by Liang [25]. In order to simplify the analysis, only a single channel in the streamwise direction will be considered in the heat exchanger, taking advantage of the periodicity in the other two dimensions. The length of the channel will be determined by repeating three unit cells, with extruded extremities created to serve as transition channels for the two fluids. All the geometrical information relevant to the topologies tested in this study is presented in Table 2. Additionally, Table 2 includes details about the different characteristic lengths, namely the pore diameter and the hydraulic diameter, that will be thoroughly discussed in Section 3.1.

### 2.3. Model and boundary conditions

The commercial software ANSYS CFX 21.1 was used to perform the numerical simulations, solving the compressible and steady-state form of continuity Eq. (4), momentum Eq. (5) and energy (Eq. (7) for the fluid phase, Eq. (8) for the solid phase) governing equations for the conjugate heat transfer process here below presented [30].

$$\nabla \cdot (\rho \mathbf{w}) = 0 \quad (4)$$

$$\nabla \cdot (\rho \mathbf{w} \otimes \mathbf{w}) = -\nabla p + \nabla \cdot \boldsymbol{\tau} \quad (5)$$

where  $\boldsymbol{\tau}$  is the stress tensor calculated as:

$$\boldsymbol{\tau} = (\mu + \mu_t) \left( \nabla \mathbf{w} + (\nabla \mathbf{w})^T - \frac{2}{3} \delta \nabla \cdot \mathbf{w} \right) + \nabla \cdot \boldsymbol{\Pi} \quad (6)$$

Table 2  
Geometrical parameters.

TPMS	Unit cell length [mm]	Thickness [mm]	Porosity [%]	Pore diameter [mm]	Hydraulic diameter [mm]
Gyroid	16	2.45	70	6.70	7.66
		1.6	81	7.0	8.62
		0.8	90	7.38	9.32
	8	0.8	81	3.62	4.20
		0.45	90	3.85	4.56
Primitive	16	1.4	70	5.12	10.02
		0.9	80	6.13	11.34
		0.5	90	6.85	12.27
	8	0.45	80	3.13	5.58
Diamond	16	2.1	70	6.56	6.06
		1.4	80	7.00	6.86
		0.75	90	7.42	7.38
	8	0.7	80	3.57	3.41

and  $\boldsymbol{\Pi}$  is the Reynolds stress tensor.

$$\nabla \cdot (\rho \mathbf{w} \mathbf{h}_{tot}) = \nabla \cdot (\lambda \nabla T) + \nabla \cdot (\mathbf{w} \cdot \boldsymbol{\tau}) \quad (7)$$

$$\lambda_s \nabla^2 T = 0 \quad (8)$$

Based on the existing literature [21], the selected turbulence model for this study is the k- $\omega$  Shear Stress Transport (SST) model, which is generally considered to offer simulation accuracy when capturing recirculations and separation zones, compared to other turbulence models.

Mass-flow rates boundary conditions are applied at the fluid inlets, while pressure boundary conditions are imposed at the fluid outlets. These boundary conditions are chosen to ensure that the simulations are well-posed and robust [30]. The inlet and outlet temperatures and the outlet pressure are kept constant for all cases. On the other hand, the mass-flow rate is intentionally varied to explore a wide range of Reynolds numbers, the ranges investigated are presented in Table 3. As previously mentioned, to improve numerical stability and minimize recirculation issues in the outlet regions, transition channels are included at the entrance regions of the computational domain (Fig. 2a).

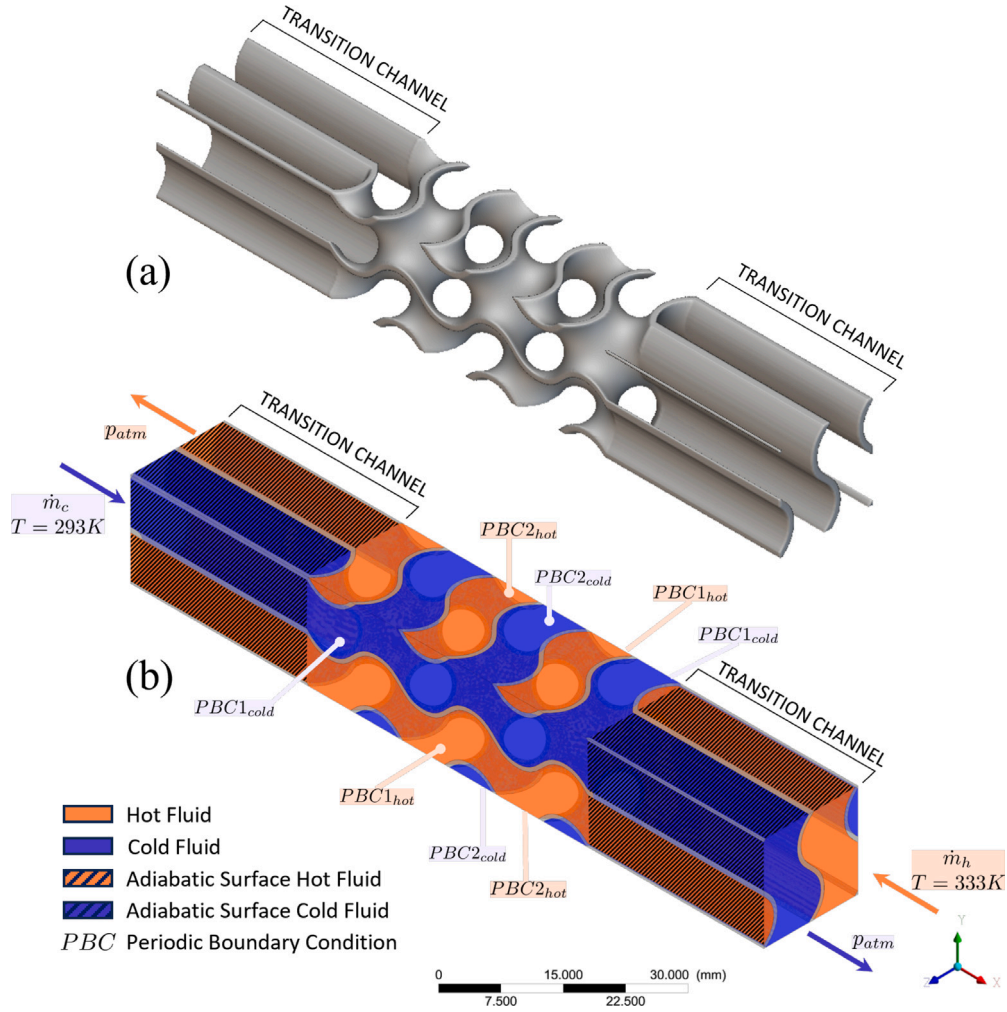


Fig. 2. Computational domain. (a) Geometry of the solid material and (b) fluid domains with summary of the boundary conditions.

**Table 3**  
Boundary conditions of fluid channels.

Fluid	Hot inlet temperature [K]	Cold inlet temperature [K]	Outlet pressure	Mass-flow rate [kg/s]
Air	333	293	1 atm	$5.85e^{-4} \div 4.54e^{-3}$
Water	333	293	1 atm	$2.59e^{-3} \div 1.64e^{-1}$
Acetone	333	293	1 atm	$1.3e^{-2} \div 8.4e^{-2}$

The transition channel at the inlet facilitates the smooth development of the flow by providing a gradual transition from the inlet to the main channel, to ensure a well-defined flow profile. The transition channel at the outlet helps to mitigate the occurrence of back-flow recirculation caused by turbulent eddies near the outlet: such recirculation may lead to numerical instability and impact the convergence of the simulation. The wall of the transition channels is set to be adiabatic, meaning that no heat transfer occurs across these channel. This choice ensures that the thermal characteristics of the transition channels do not affect the heat transfer behavior within the TPMS domain of interest, allowing for accurate analysis and interpretation of the results. For the fluid-solid interfaces, a general coupling condition is enforced, ensuring the conservation of heat flux in the TPMS region. Thanks to the periodic nature of such heat exchangers, periodic boundary conditions are applied to the top, bottom and sides of the domain. This approach effectively reduces the size of the domain, thus limiting the computational cost

associated with the simulations. The boundary conditions of the model are summarized in Fig. 2b.

#### 2.4. Mesh

To adequately represent the complex geometries of TPMS lattice structures, unstructured meshes are employed for discretizing both the fluid and solid domains. The commercial software ANSYS ICEM 2021 is used for this purpose. In order to accurately capture the thermal and velocity boundary layers, a total of 24 prism layers are employed. These layers grow with a ratio of 1.21 from an initial layer thickness of 0.0005 mm (Fig. 3). This configuration ensures that the non-dimensional wall distance  $y^+$  remains below 1, which is crucial for obtaining accurate results when using the  $k-\omega$  SST turbulence model. To optimize computational efficiency, coarser tetrahedral meshes are implemented in regions located away from the boundary layer.

#### 2.5. Computational model validation

Prior to conducting simulations for the development of the heat transfer correlation, it is necessary to validate the previously presented numerical model. Liang [25] conducted a study where the values of the overall heat transfer coefficient per unit surface ( $U$ ) for experimentally tested TPMS heat exchangers were reported, along with corresponding numerical simulations. The overall heat transfer coefficient per unit surface of the heat exchanger is obtained using Eq. (9):

$$U = \frac{\dot{Q}}{LMTD \cdot A_{HX}} \quad (9)$$



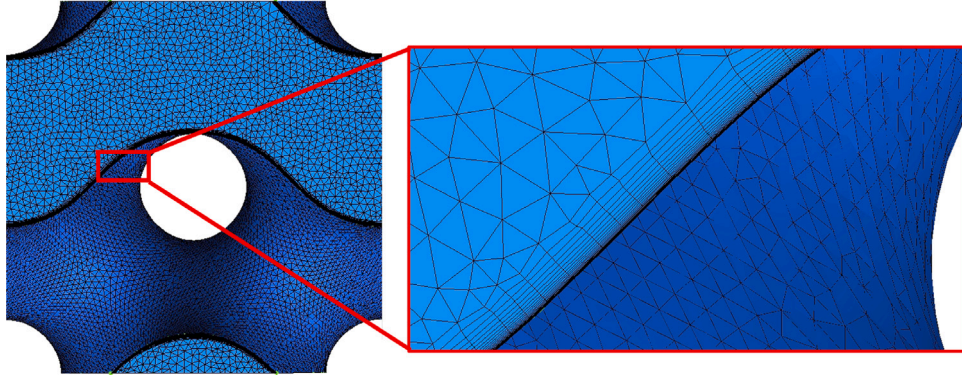


Fig. 3. Mesh on a fluid domain and zoom to highlight the prism layers.

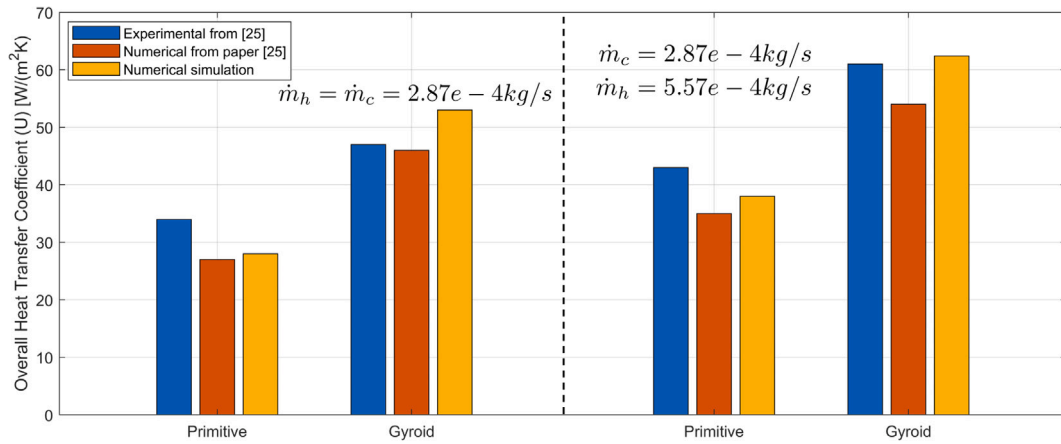


Fig. 4. Overall heat transfer coefficient comparison between the numerical result of the present CFD simulations and both the experimental and numerical ones presented in [25].

Therefore, the first simulations performed for this work are aimed to replicate the results from [25]. The working fluid is air and it is modeled using ideal gas assumption and constant thermophysical properties, reported in Table 1. The mass-flow rates are specified to replicate the experimental setup. The results of such simulations are presented in Fig. 4. In line with the numerical simulations conducted in [25], the maximum deviation observed between the experimental and numerical overall heat transfer coefficient (U) values is found to be less than 18%. This level of deviation indicates that the numerical model provides a good representation of the physical phenomena occurring within the heat exchanger. Additionally, it is worth noting that the experimental results reported in [25] have themselves an associated uncertainty of approximately 7%. In Table 4 are presented the results of the mesh-independence study, where the case of Gyroid with unbalanced mass-flow rates [25], i.e. two different values of mass-flow rates for the two fluid domains, is considered. The total number of cells is determined to be approximately 20 million, composed by 9.5 millions cells for each of the two fluid domains and 1 million for the solid one.

Furthermore, simulations have been performed on a channel composed by 6 cells to investigate the potential scaling effect. The results reveal that the numerical outcomes for the 3 cells and 6 cells cases differ by less than 1%, for the value of U. All these results demonstrate that the current numerical method and turbulence model are capable of providing accurate data for heat transfer analysis, as the observed differences are within an acceptable range.

### 3. Correlation calibration and validation

#### 3.1. Non-dimensional analysis

The objective of this research is to develop a single correlation capable of accurately predicting the convective heat transfer coefficient

Table 4

Results of the mesh-independence study. Experimental value from [25].  $\Delta$  defined as the deviation from the result of the 10 million cells simulation.

Million cells	$U_{CFD}$ [W/m²K]	$\Delta$ [%]	$U_{Exp}$ [W/m²K]
10	63.15	–	60.7
20	62.14	1.6	
40	62.09	1.7	

for different fluids and various TPMS geometries. The correlation that will be investigated is based upon the Dittus-Boelter correlation [1]. As it combines simplicity with the presence of three coefficients available for the fitting, such correlation was preferred to others, also considered more sophisticated and accurate, as for the example of the well known Gnielinski correlation [1]. The Dittus-Boelter correlation is a power-law in the form:

$$Nu = A Re^m Pr^{n(h,c)} \quad (10)$$

where  $Nu$ ,  $Re$  and  $Pr$  are non-dimensional groups and  $A$ ,  $m$  and  $n_{(h,c)}$  are the parameters that have to be fitted. To introduce an additional degree of freedom, distinct exponents for the Prandtl number are initially taken into account for the hot ( $n_h$ ) and cold ( $n_c$ ) fluids. Three non-dimensional groups are chosen to reduce the variables of the problem at hand. Nusselt number ( $Nu$ ) is used to quantify heat transfer by convection and the heat transfer enhancement due to fluid motion. It is calculated as

$$Nu = \frac{h L}{\lambda} \quad (11)$$

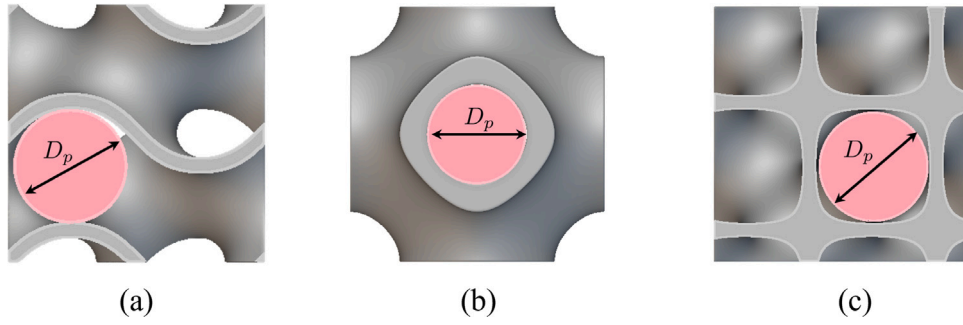


Fig. 5. Pore diameter for the three topologies considered. (a) Gyroid, (b) Schwarz-Primitive, (c) Schwarz-Diamond.

Reynolds number ( $Re$ ) is used to describe the fluid flow characteristics and it is defined as:

$$Re = \frac{\rho W_p L}{\mu} \quad (12)$$

Concerning the thermo-physical properties of the fluids, these are adimensionalized using the Prandtl number, defined as:

$$Pr = \frac{c_p \mu}{\lambda}. \quad (13)$$

For complex geometries, the selection of the characteristic length ( $L$ ) may be non trivial and much less straightforward than in the classic cases as flat surfaces and cylinders or spheres, requiring careful consideration on the physics of the phenomena of interest. Due to the non-uniform cross-section of the channels created by TPMS structures, the fluid undergoes accelerations and decelerations along its path. Therefore, for the computation of the Reynolds number, the characteristic length chosen for this work is the equivalent pore diameter ( $D_p$ ), computed as the diameter of the largest sphere that can be inscribed in the structure (Fig. 5). The velocity considered in the Reynolds computation is the average value over the pore area computed where the velocity reaches its maximum value, so as to have an indication of the maximum Reynolds attained within the geometry. This choice is often used in the literature when dealing with open-cells regular structures [22], [18]. To compute the value of the pore diameter, the open-source software *ImageJ* [31] is used, and in particular the *Thickness* feature, that is able to compute the diameter of the largest sphere that fits within the structure.

A preliminary analysis of the results revealed that selecting the pore diameter as the characteristic length also for the Nusselt number does not yield a unique correlation for both Gyroid and Schwarz-Primitive. The Gyroid structure, for all Reynolds number values, produces significantly higher Nusselt numbers compared to the Schwarz-Primitive. This observation aligns with previous studies in the literature [25], which attribute the differences to the distinct flow paths generated by the two structures. This can be visually seen in Fig. 6, where the streamlines of the three different topologies are presented together with two cross-sectional slices of the domain showing the flow vorticity. In the Schwarz-Primitive structure, a large part of the fluid flow follows a straight path along the central tunnel of the TPMS structure, while the side parts of the cell volume are characterized by significant stagnation regions. This negatively affects the heat exchange performance. In contrast, the fluid flows with much larger and more uniform velocity in the Gyroid and Schwarz-Diamond structures. In addition, the fluid exhibits a more intricate flow pattern, involving continuous changes in direction. This complexity induces large-scale bifurcation flow, intensifying interaction with the wall and enhancing the overall exchange between the fluid and solid surfaces. A more detailed description of the fluid flow characteristics of these different topologies can be found in [25].

The disparity in Nusselt numbers between Gyroid and Schwarz-Primitive can also be attributed to the fact that the pore diameter lacks a direct physical relation with the heat transfer phenomenon. To

address this issue, an investigation into using different characteristic lengths exclusively for the Nusselt number was conducted and the choice fell upon the hydraulic diameter ( $D_h$ ). In the context of complex geometries, the hydraulic diameter serves as a measure of the heat exchange area in relation to the volume of the channel. Hydraulic diameter is computed as [32]:

$$D_h = \frac{4 V}{A_{HX}} \quad (14)$$

### 3.2. Convective heat transfer coefficient computation

Initially, the convective heat transfer coefficient is treated as a local parameter, and its computation involves the following steps. Firstly, the bulk temperature of the fluid domain needs to be determined. To achieve this, from the results of the CFD simulations the domain of each fluid is discretized into multiple cross-sections along the length of the channel. For each cross-section, the adiabatic-cup mixing temperature [1] is computed using the formula:

$$T_b(x) = \frac{\int_{A_c} \rho c_p \mathbf{w} T dA_c}{\dot{m} c_p} \quad (15)$$

Subsequently, the bulk temperature of the fluid domain ( $T_b$ ) is obtained as the mean average of the adiabatic-cup mixing temperatures calculated across the various cross-sections. Once the bulk temperature of the fluid is defined, the local convective heat transfer coefficient is calculated using Newton's law:

$$h_{local} = \frac{\dot{Q}''}{(T_{wall} - T_b)} \quad (16)$$

The value of the convective heat transfer coefficient that will be considered is the average of the local values over the heat exchange area.

### 3.3. Correlation calibration

To obtain the correlation, a total of 13 simulations were conducted, encompassing two different Reynolds numbers for each domain. During this phase, the simulations were performed using two types of fluids, namely air and liquid water, with thermo-physical properties provided in Table 1. The selection of these fluids was deliberate, aiming to develop a correlation that remains valid across a range of Prandtl numbers between 0.7 and 7, which corresponds to the typical Prandtl number range for most fluids. To introduce variations in the Reynolds number, adjustments were made to the mass-flow rate at the inlet of the channel. The range of Reynolds numbers examined spanned from 5000 to 50000, covering typical values of turbulent flow regime. Subsequently, the values of the convective heat transfer coefficient obtained from the CFD analysis were fitted with a least square minimization approach.

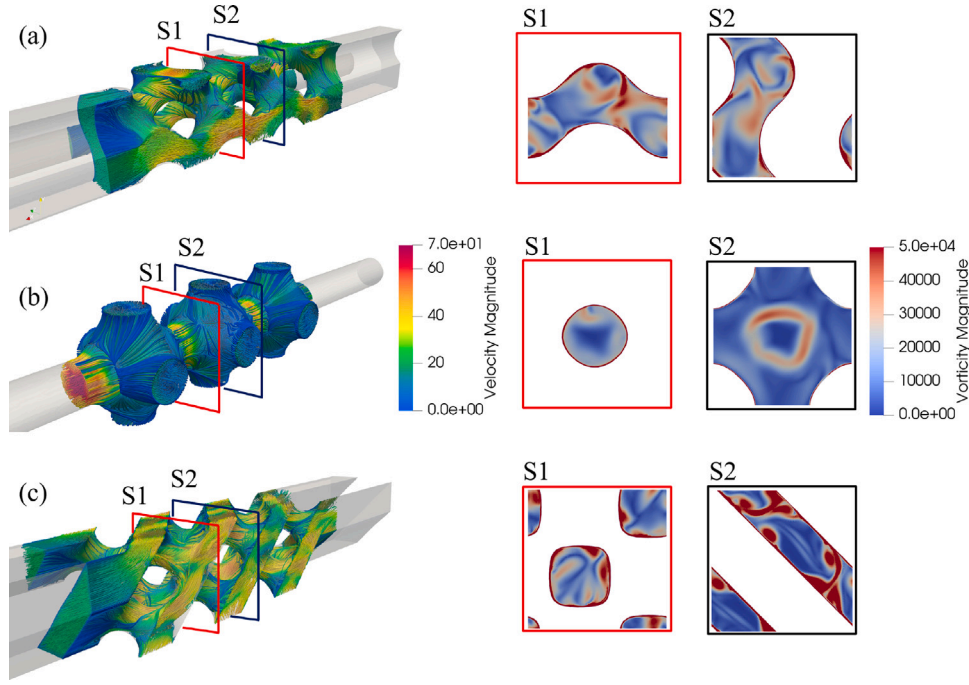


Fig. 6. 3D streamlines for the three different topologies and vorticity on two planes perpendicular to the stream direction. (a) Gyroid, (b) Schwarz-Primitive, (c) Schwarz-Diamond.  $Re = 20000$ , hot air.

### 3.4. Correlation validation

Once the correlation parameters have been fitted, it is necessary to validate the correlation against various test cases. As mentioned earlier, the primary objective of this study is to identify a single correlation that can be universally applied to different TPMS structures and fluids. To accomplish this, the first step involves validating the correlation using a different fluid, while maintaining the same geometry used during the calibration process. Acetone was chosen for this validation since its Prandtl values lie in the middle of the selected Prandtl number's range (0.7–7). The thermo-physical properties of acetone are detailed in Table 1.

Schwarz-Primitive and Schwarz-Diamond are the topologies chosen in order to assess the validity of the correlation against different topologies. Simulations were also conducted for the three topologies using two additional porosity values, specifically 70% and 90%, while maintaining a constant cell unit length. Consequently, simulations have been performed also considering topologies with 8 mm as unit length and a 80% porosity value. For the case of Gyroid only, simulations were performed considering 8 mm unit length and 90% porosity. The results are presented in Section 4.2, where the effect of the different cases, namely different fluids, different topologies and different geometrical values will be highlighted.

## 4. Results and discussion

### 4.1. Calibration

The results of the calibration are shown in Fig. 7, where the correlation with the relative error bands are the continuous lines while the CFD results the single points. In Fig. 7, the y-axis represents the Nusselt number divided by the Prandtl number raised to the exponent for the corresponding cold/hot fluid. This choice of representation aims to provide a clearer visualization of the correlation's dependency on the Reynolds number, independently of the specific fluid being considered. Upon careful examination of Fig. 7, it is evident that only 20% of the results (5 out of 24) deviate beyond the  $\pm 10\%$  range from the correlation. This outcome is considered satisfactory, as it indicates that

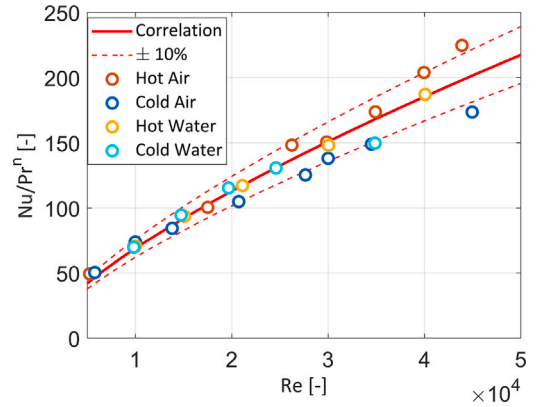


Fig. 7. Correlation calibration.

Table 5

Correlation results.

A	m	$n_{(h,c)}$
0.0964	0.7136	0.4

the correlation chosen (Eq. (10)) is adequate to represent the results obtained from the CFD simulations. As the numerical parameter fitting resulted in values for  $n_h$  and  $n_c$  that are very similar to each other ( $n_h = 0.399$  and  $n_c = 0.393$ ), it was decided to adopt a single value of 0.4 for the exponent. The final coefficients for the proposed correlation are summarized in Table 5.

### 4.2. Validation

#### 4.2.1. Effect of different fluids

As discussed in Section 3.4, the developed correlation was initially validated using results obtained from simulations with acetone. Fig. 8 illustrates the validation results for the case of Gyroid used for the calibration, demonstrating that all tested cases fall within the  $\pm 10\%$

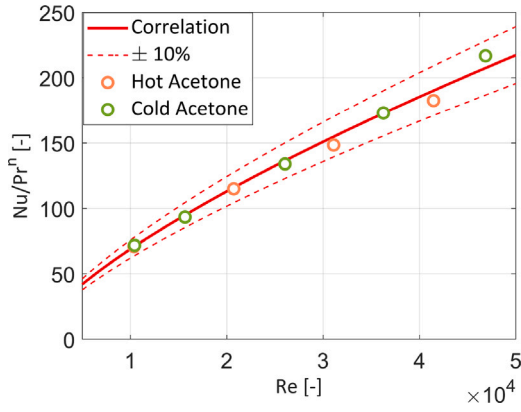


Fig. 8. Validation of the proposed correlation with a different fluid (acetone). Gyroid topology, 16 mm unit cell length and 80% porosity.

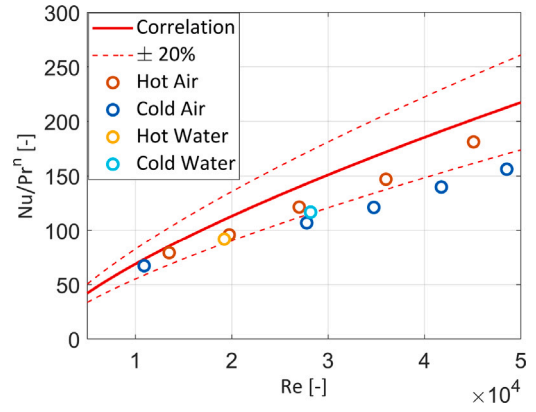


Fig. 10. CFD results and correlation prediction for the case of Schwarz-Diamond topology. Unit cell length 16 mm and 80% porosity.

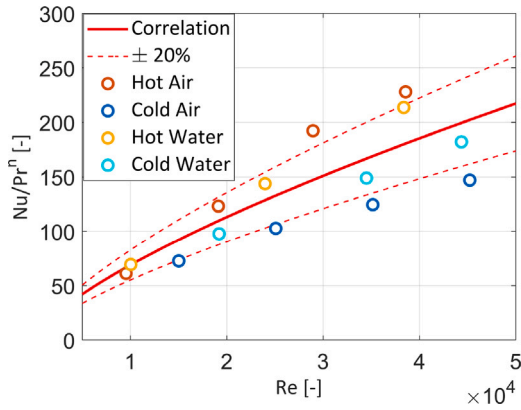


Fig. 9. CFD results and correlation prediction for the Schwarz-Primitive topology. Unit cell length 16 mm and 80% porosity.

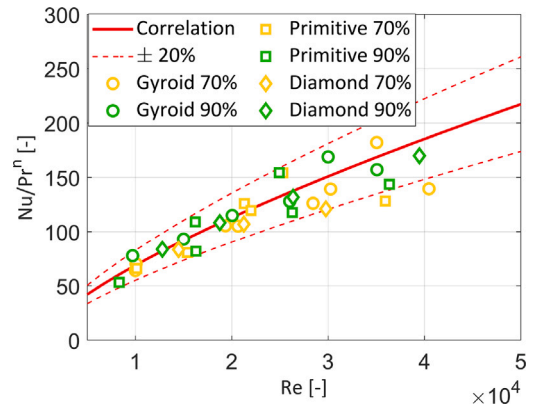


Fig. 11. CFD results and correlation prediction for the three topologies with porosity 70% and 90%. Unit cell length 16 mm.

scatter band of the correlation. This successful outcome indicates the predictive capability of the correlation when applied to different fluids.

#### 4.2.2. Effect of different topologies

Following the successful validation of the correlation using a different fluid, further simulations were performed on different topologies. This investigation aimed to assess whether the proposed correlation could accurately predict the convective heat transfer coefficient for different TPMS geometries. The results for the Schwarz-Primitive are illustrated in Fig. 9. In contrast to the Gyroid case, the results exhibit a more scattered distribution. This variation in the results is attributed to the influence of viscous work terms on the computation of the convective heat transfer coefficient, a topic that will be further addressed in Section 4.3. Despite the dispersion of the results, the proposed correlation effectively captures the overall trend observed in the simulations. With a scatter band of  $\pm 20\%$  applied to the predicted values, 64% of the simulated data points (9 out of 14) fall within the designated range, indicating a reliable predictive capability of the correlation.

The results of the Schwarz-Diamond topology are presented in Fig. 10. Differently from the previous cases, the proposed correlation exhibits a systematic overestimation of the convective heat transfer coefficient for this topology. This observation is attributed to the outstanding thermal performances of the Schwarz-Diamond topology, that is able to generate a strong turbulent flow, resulting in high convective heat transfer coefficients, comparable to those obtained for the Gyroid topology, while being characterized by a large heat exchange surface

and a significantly lower value of hydraulic diameter compared to the Gyroid topology (as shown in Table 2). This difference in hydraulic diameter contributes to the lower values of Nusselt numbers observed for the Schwarz-Diamond structure. Despite the observed differences, it is noteworthy that the majority of the CFD results still fall within the 20% scatter band of the proposed correlation. This outcome demonstrates the correlation's general validity and its ability to reasonably predict the convective heat transfer coefficients for a wide range of TPMS structures.

#### 4.2.3. Effect of geometrical parameters

Having successfully validated the correlation for different TPMS topologies, the next step involves testing its applicability to variations in the geometry parameters, such as porosity and unit cell length. This investigation aims to determine if the chosen characteristic length can effectively capture the underlying physical phenomena of interest across different geometries. Given that the correlation was calibrated using results from an 80% porous cell, its validation investigated cells with 70% and 90% porosity, to assess the correlation's performance across a typical range of porosity values commonly encountered in TPMS structures [19]. Fig. 11 presents the results for the three topologies, respectively for 70% and 90% porous structures. As it can be seen, the correlation is able to predict the convective heat transfer coefficient considering deviations of the order of  $\pm 20\%$ .

Concerning the correlation's applicability to geometries with different unit cell length, a series of simulations were conducted on the three topologies with an 8 mm unit cell length, which is half the value used for calibration. As the correlation has already demonstrated



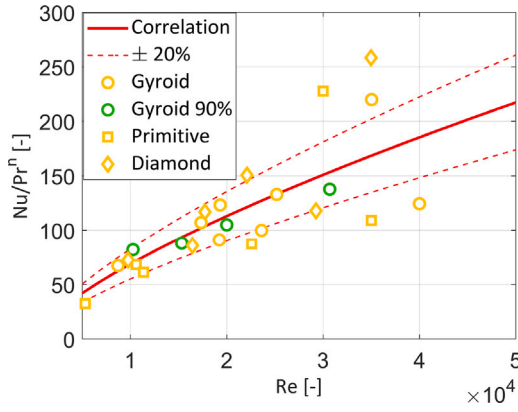


Fig. 12. CFD results and correlation prediction for TPMS with unit cell length of 8 mm. Porosity value 80% for all cases except for one case with Gyroid at 90%.

its porosity-independence, a structure with 80% porosity was chosen to maintain consistency with the calibration case. In addition, a case with both unit cell length and porosity different from the calibration was tested. The results of these simulations are presented in Fig. 12, confirming the correlation's ability to accurately predict the convective heat transfer coefficient also for TPMS structures with different unit cell length. Fig. 12 also reveals that points exceeding a 20% error are noticeable at Reynolds numbers lower than those observed for the 16 mm cells, this points out that viscous effects (discussed extensively in Section 4.3), are more relevant on smaller cells. What emerges from Figs. 11 and 12 is that the proposed correlation is suitable to predict the convective heat transfer coefficient at various Reynolds numbers, for different topologies, with different geometrical parameters.

#### 4.3. Viscous effects and total temperature correlation

In Fig. 7, it can be noted that at high Reynolds the values for the hot and cold fluid start to diverge, especially for the case of air. This divergence is primarily attributed to the phenomenon of viscous heating in regions with high wall shear stress. In such areas, the wall temperature ( $T_{wall}$ ) experiences a substantial increase. Thus, the denominator of Eq. (16) will decrease for the case of hot fluid ( $T_b > T_{wall}$ ) and increase for the case of cold fluid ( $T_b < T_{wall}$ ). Imposing the same heat flux for the two domain, this will lead to the increase of the local convective heat transfer coefficient of the hot fluid and a decrease in the cold one. In Fig. 13, the outcomes of two CFD simulations are presented, illustrating the comparison between cases with and without including viscous work terms in the energy equation for hot air. The relevance of this effect in the average value of the convective

Table 6

Correlation results considering total temperature.

A	m	$n_h$	$n_c$
0.0964	0.7136	0.40	0.38

heat transfer coefficient can be understood thanks to the Reynold's analogy [33]. In fluid flow over a solid surface, two key processes occur: the transfer of momentum due to the flow velocity (momentum transfer) and the transfer of heat due to temperature differences (heat transfer). Reynolds' analogy suggests that there is a direct relationship between these two processes, meaning that the rate of heat transfer can be related to the rate of momentum transfer. Mathematically, Reynolds' analogy can be expressed as:

$$\dot{Q}'' \approx \frac{\tau_w c_p (T_{wall} - T_b)}{W_b} \quad (17)$$

Consequently, regions characterized by high wall shear stress will exhibit significant heat transfer, influencing the overall average value of the convective heat transfer coefficient. This effect is particularly pronounced in the case of Schwarz-Primitive due to the fact that, out of the regions with high wall shear stress, the convective heat transfer coefficient across the remaining heat exchange surface is relatively low, impacting the average value of the coefficient (Fig. 14). The other topologies are instead able to generate high flow-mixing that increase the interaction between the fluid and the solid wall leading to more uniform value of the convective heat transfer coefficient across the whole heat exchange surface. This reduce the effect of the viscous heating with respect of the Schwarz-Primitive case.

In scenarios involving high-speed flows, the total temperature defined as Eq. (18) is commonly employed to account for the effects of viscous heating [34]. In such cases, the total temperature is used in determining the bulk temperature of the fluid for Eq. (16). Although this approach is less common in the design of heat exchangers, which typically focus on low-speed flows, for the sake of completeness, the results, along with the associated correlation parameters considering the total temperature, are presented in Figs. 15, 16, 17 and Table 6. As it can be noted, the correlation parameters are highly similar to the one estimated using the static temperature. However, especially from Fig. 16, the results at high Reynolds numbers are more close to the ones estimated by the correlations.

$$T_0 = T + \frac{W^2}{2 c_p} \quad (18)$$

#### 4.4. Comparison with existing correlations

Since the new correlation was derived from the original Dittus-Boelter correlation, a comparative analysis was conducted between the

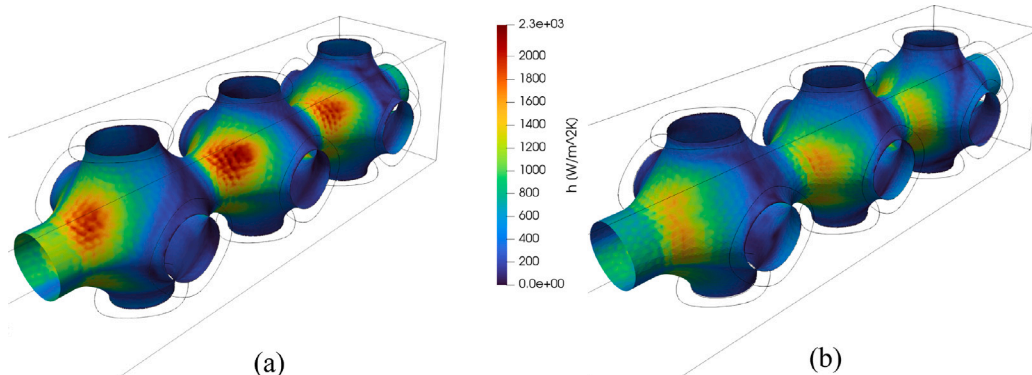


Fig. 13. Distribution of the local convective heat transfer coefficient for the Schwarz-Primitive topology considering the viscous work term in the energy equation (a) and neglecting the viscous work terms (b).

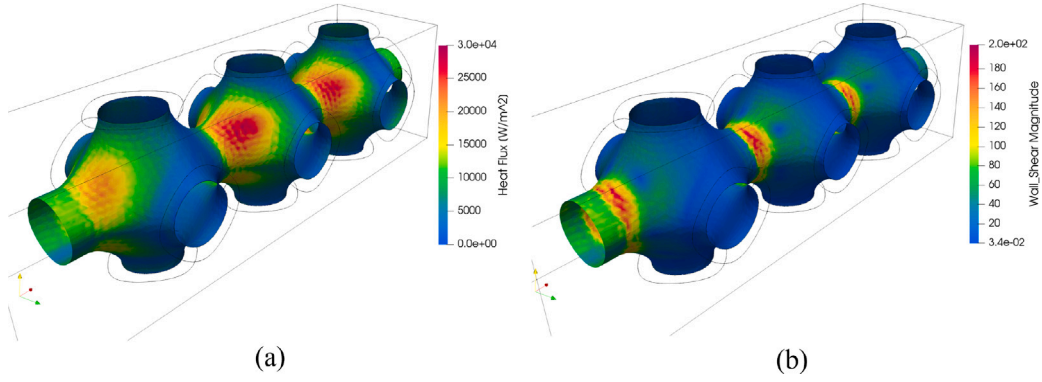


Fig. 14. Reynolds analogy in Schwarz-Primitive topology. (a) heat flux, (b) wall shear stress.

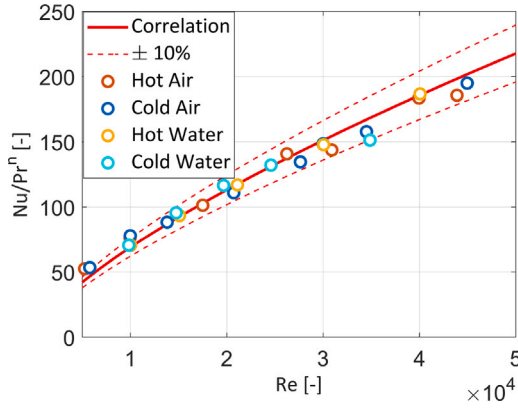


Fig. 15. Correlation calibration using the total temperature.

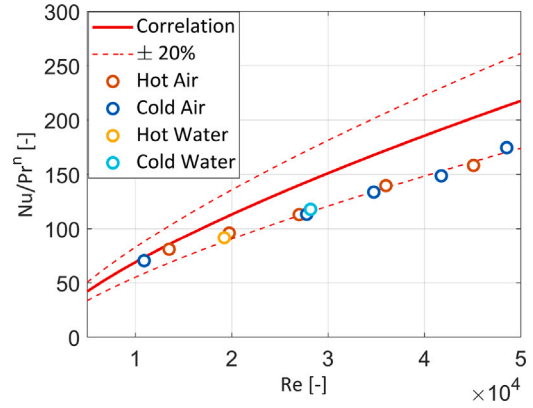


Fig. 17. CFD results and correlation prediction for Schwarz-Diamond topology using the total temperature.

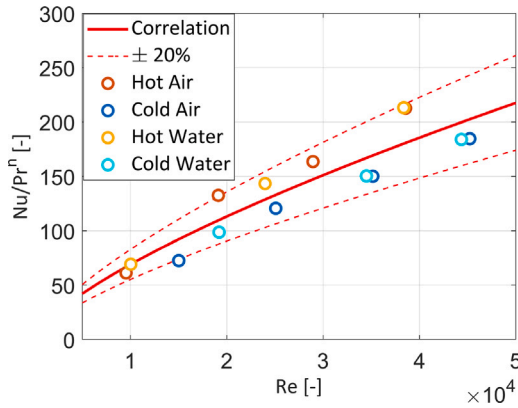


Fig. 16. CFD results and correlation prediction for Schwarz-Primitive topology using the total temperature.

outcomes of the newly developed correlation and the results that would be obtained using the original Dittus-Boelter correlation (Eq. (19)). Furthermore, the Gnielinski correlation (Eq. (20)) was included in the comparison, as it is widely recognized as one of the most effective for predicting convective heat transfer coefficients. This aims to provide the readers with quantitative insights into the underestimation associated with traditional correlations when applied in the context of TPMS structures. Furthermore, this article's proposed correlation has been subjected to comparison with a correlation sourced from the literature [24] and showed in Eq. (21). The presented results, illustrated in Fig. 18, are related only to the gyroid case, as the correlation in [24]

specifically applies to this topology and for air as the working fluid.

$$Nu_D = 0.023 Re_D^{0.8} Pr^n, \text{ with } \begin{cases} n = 0.4 & \text{for the fluid being heated} \\ n = 0.3 & \text{for the fluid being cooled} \end{cases} \quad (19)$$

$$Nu_D = \frac{(f/8)(Re_D - 1000)Pr}{1 + 12.7(f/8)^{1/8}(Pr^{2/3} - 1)} \quad (20)$$

$$Nu_{D_h} = 0.49 Re_{D_h}^{0.62} Pr^{0.4} \text{ for } 100 < Re < 2500 \quad (21)$$

Fig. 18 illustrates the disparities between a perfect correlation (continuous black line) and the results obtained with the new correlation, the two aforementioned classic correlations. Upon examination, it becomes apparent that the two traditional correlations systematically underestimate the convective heat transfer coefficient, resulting in deviations ranging from 20% to 60% when compared to the values computed from CFD simulations. From 18, it is possible to appreciate that the correlation in [24] tends to overestimate the convective heat transfer coefficient by a factor of 2 when compared to the CFD results. This discrepancy can be attributed to the fact that the correlation in [24] is applicable to a lower range of Reynolds numbers ( $Re < 2500$ ). In contrast, the newly developed correlation is able to predict the convective heat transfer coefficient with more accuracy, being the majority of the results inside a  $\pm 20\%$  error band.

## 5. Conclusions

Researchers have recognized the unique characteristics and potential of TPMS structures for enhancing heat transfer in various applications. The growing interest in TPMS structures highlights the importance of exploring their heat transfer characteristics for the design of highly efficient and compact heat exchangers. The results of this

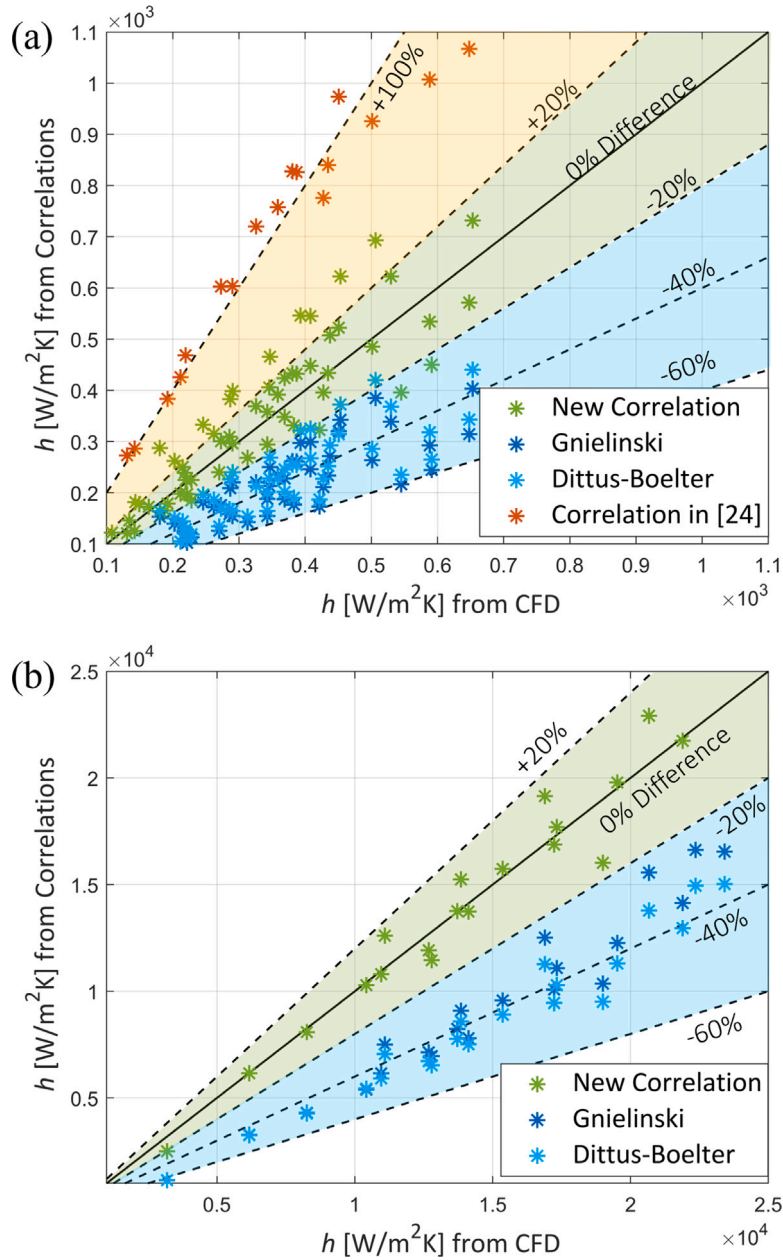


Fig. 18. Comparison of CFD values of convective heat transfer coefficient with those predicted by the new correlation, the Dittus-Boelter, the Gnielinski and the one proposed in [24]. In (a) the fluid considered is air, in (b) the fluid considered is water.

study indicate that it is possible to formulate a single heat transfer correlation that is able to capture the convective heat transfer coefficient:

- for different TPMS structure (Gyroid, Schwarz-Primitive and Schwarz-Diamond)
- for fully turbulent flow regime (Reynolds number from 5000 to 50000)
- for different fluids (with a Prandtl number from 0.7 to 7)
- for different values of unit cell size and porosity

This study also evidenced the influence of viscous work terms on the convective heat transfer coefficient for the different topologies. Notably, among the three tested, the Schwarz-Primitive topology experiences the greatest impact from this phenomenon. In addition the proposed correlation has been compared with traditional correlations, in order to quantify their underestimation when dealing with TPMS structures. Furthermore, comparisons were made with correlations for

TPMS structures from existing literature. The outcomes of these comparisons emphasize the improved accuracy of the proposed correlation in alignment with the results obtained from the CFD analysis. To further address this aspect, a modified version of the correlation, based on the total temperature instead of the static temperature, was also developed and tested, showing improved performances for high-speed cases.

Further studies will have to focus on:

- the experimental validation of the proposed correlation
- a single correlation that is valid for pressure drops evaluation
- the mechanical resistance of TPMS structures under thermal loads and thermal cycles

By addressing these aspects, the proposed correlation can be further reinforced and validated for a wide range of practical applications and also completed with additional important information about the thermo-fluid dynamic behavior, thus enabling more efficient and accurate design of heat exchangers based on TPMS structures.

## CRediT authorship contribution statement

**Giovanni Brambati:** Writing – original draft, Software, Investigation, Data curation, Conceptualization. **Manfredo Guilizzoni:** Writing – review & editing, Supervision, Software, Conceptualization. **Stefano Foletti:** Writing – review & editing, Supervision, Resources, Project administration.

## Declaration of competing interest

The authors declare that they have no known competing financial interests or personal relationships that could have appeared to influence the work reported in this paper.

## Data availability

Data will be made available on request.

## Acknowledgments

Giovanni Brambati acknowledges funding from FSE REACT-EU, Programma Operativo Nazionale Ricerca e Innovazione 2014–2020 (CCI2014IT16M2OP005), Azione IV.5 “Dottorati su tematiche Green” (DOT1316301-12).

## References

- [1] F.P. Incropera, D.P. DeWitt, T.L. Bergman, A.S. Lavine, et al., *Fundamentals of Heat and Mass Transfer*, Vol. 6, Wiley, New York, 1996.
- [2] Q. Li, G. Flamant, X. Yuan, P. Neveu, L. Luo, Compact heat exchangers: A review and future applications for a new generation of high temperature solar receivers, *Renew. Sustain. Energy Rev.* 15 (9) (2011) 4855–4875, <http://dx.doi.org/10.1016/j.rser.2011.07.066>.
- [3] F. Careri, R.H. Khan, C. Todd, M.M. Attallah, Additive manufacturing of heat exchangers in aerospace applications: a review, *Appl. Therm. Eng.* 235 (2023) 121387, <http://dx.doi.org/10.1016/j.applthermaleng.2023.121387>, URL: <https://www.sciencedirect.com/science/article/pii/S1359431123014163>.
- [4] A. Fawaz, Y. Hua, S. Le Corre, Y. Fan, L. Luo, Topology optimization of heat exchangers: A review, *Energy* 252 (2022) 124053, <http://dx.doi.org/10.1016/j.energy.2022.124053>.
- [5] I. Kaur, P. Singh, State-of-the-art in heat exchanger additive manufacturing, *Int. J. Heat Mass Transfer* 178 (2021) <http://dx.doi.org/10.1016/j.ijheatmasstransfer.2021.121600>.
- [6] T.A. Schaedler, W.B. Carter, Architected cellular materials, *Annu. Rev. Mater. Res.* 46 (1) (2016) 187–210, <http://dx.doi.org/10.1146/annurev-matsci-070115-031624>.
- [7] K.J. Maloney, K.D. Fink, T.A. Schaedler, J.A. Kolodziejska, A.J. Jacobsen, C.S. Roper, Multifunctional heat exchangers derived from three-dimensional micro-lattice structures, *Int. J. Heat Mass Transfer* 55 (9) (2012) 2486–2493, <http://dx.doi.org/10.1016/j.ijheatmasstransfer.2012.01.011>.
- [8] Y. Aider, I. Kaur, H. Cho, P. Singh, Periodic heat transfer characteristics of additively manufactured lattices, *Int. J. Heat Mass Transfer* 189 (2022) <http://dx.doi.org/10.1016/j.ijheatmasstransfer.2022.122692>.
- [9] E. Bianchi, W. Schwieger, H. Freund, Assessment of periodic open cellular structures for enhanced heat conduction in catalytic fixed-bed reactors, *Adv. Eng. Mater.* 18 (4) (2016) 608–614, <http://dx.doi.org/10.1002/adem.201500356>.
- [10] C. Ferroni, M. Bracconi, M. Ambrosetti, M. Maestri, G. Groppi, E. Tronconi, A fundamental investigation of gas/solid heat and mass transfer in structured catalysts based on periodic open cellular structures (POCS), *Ind. Eng. Chem. Res.* 60 (2021) 10522–10538, <http://dx.doi.org/10.1021/acs.iecr.1c00215>.
- [11] A. Kopanidis, A. Theodorakakos, E. Gavaises, D. Bouris, 3D numerical simulation of flow and conjugate heat transfer through a pore scale model of high porosity open cell metal foam, *Int. J. Heat Mass Transfer* 53 (11) (2010) 2539–2550, <http://dx.doi.org/10.1016/j.ijheatmasstransfer.2009.12.067>.
- [12] J. Feng, J. Fu, X. Yao, Y. He, Triply periodic minimal surface (TPMS) porous structures: from multi-scale design, precise additive manufacturing to multi-disciplinary applications, *Int. J. Extrem. Manuf.* 4 (2) (2022) 022001, <http://dx.doi.org/10.1088/2631-7990/ac5be6>.
- [13] K. Yeranee, Y. Rao, A review of recent investigations on flow and heat transfer enhancement in cooling channels embedded with triply periodic minimal surfaces (TPMS), *Energies* 15 (23) (2022) <http://dx.doi.org/10.3390/en15238994>, URL: <https://www.mdpi.com/1996-1073/15/23/8994>.
- [14] O. Al-Ketan, R.K. Abu Al-Rub, Multifunctional mechanical metamaterials based on triply periodic minimal surface lattices, *Adv. Eng. Mater.* 21 (10) (2019) 1900524, <http://dx.doi.org/10.1002/adem.201900524>.
- [15] V. Slaughter, Method of using minimal surfaces and minimal skeletons to make heat exchanger components, 2011, U.S. Patent 7, 866, 377[P]. 2011-1-11.
- [16] T. Femmer, A.J. Kuehne, M. Wessling, Estimation of the structure dependent performance of 3-D rapid prototyped membranes, *Chem. Eng. J.* 273 (2015) 438–445, <http://dx.doi.org/10.1016/j.cej.2015.03.029>.
- [17] T. Dixit, E. Al-Hajri, M.C. Paul, P. Nithiarasu, S. Kumar, High performance, microarchitected, compact heat exchanger enabled by 3D printing, *Appl. Therm. Eng.* 210 (2022) <http://dx.doi.org/10.1016/j.applthermaleng.2022.118339>.
- [18] I. Kaur, P. Singh, Flow and thermal transport characteristics of Triply-Periodic Minimal Surface (TPMS)-based gyroid and Schwarz-P cellular materials, *Numer. Heat Transfer; A: Appl.* 79 (2021) 553–569, <http://dx.doi.org/10.1080/10407782.2021.1872260>.
- [19] R. Attarzadeh, M. Rovira, C. Duwig, Design analysis of the “Schwartz D” based heat exchanger: A numerical study, *Int. J. Heat Mass Transfer* 177 (2021) <http://dx.doi.org/10.1016/j.ijheatmasstransfer.2021.121415>.
- [20] J. Iyer, T. Moore, D. Nguyen, P. Roy, J. Stolaroff, Heat transfer and pressure drop characteristics of heat exchangers based on triply periodic minimal and periodic nodal surfaces, *Appl. Therm. Eng.* 209 (2022) <http://dx.doi.org/10.1016/j.applthermaleng.2022.118192>.
- [21] W. Li, G. Yu, Z. Yu, Bioinspired heat exchangers based on triply periodic minimal surfaces for supercritical CO<sub>2</sub> cycles, *Appl. Therm. Eng.* 179 (2020) <http://dx.doi.org/10.1016/j.applthermaleng.2020.115686>.
- [22] O. Al-Ketan, M. Ali, M. Khalil, R. Rowshan, K.A. Khan, R.K.A. Al-Rub, Forced convection computational fluid dynamics analysis of architected and three-dimensional printable heat sinks based on triply periodic minimal surfaces, *J. Therm. Sci. Eng. Appl.* 13 (2021) <http://dx.doi.org/10.1115/1.4047385>.
- [23] M. Khalil, M.I.H. Ali, K.A. Khan, R.A. Al-Rub, Forced convection heat transfer in heat sinks with topologies based on triply periodic minimal surfaces, *Case Stud. Therm. Eng.* 38 (2022) <http://dx.doi.org/10.1016/j.csite.2022.102313>.
- [24] B.W. Reynolds, C.J. Fee, K.R. Morison, D.J. Holland, Characterisation of heat transfer within 3D printed TPMS heat exchangers, *Int. J. Heat Mass Transfer* 212 (2023) 124264, <http://dx.doi.org/10.1016/j.ijheatmasstransfer.2023.124264>, URL: <https://www.sciencedirect.com/science/article/pii/S0017931023004167>.
- [25] D. Liang, C. Shi, W. Li, W. Chen, M.K. Chyu, Design, flow characteristics and performance evaluation of bioinspired heat exchangers based on triply periodic minimal surfaces, *Int. J. Heat Mass Transfer* 201 (2023) <http://dx.doi.org/10.1016/j.ijheatmasstransfer.2022.123620>.
- [26] N. Baobaid, M.I. Ali, K.A. Khan, R.K.A. Al-Rub, Fluid flow and heat transfer of porous TPMS architected heat sinks in free convection environment, *Case Stud. Therm. Eng.* 33 (2022) <http://dx.doi.org/10.1016/j.csite.2022.101944>.
- [27] J. Jayakumar, S. Mahajani, J. Mandal, P. Vijayan, R. Bhoi, Experimental and CFD estimation of heat transfer in helically coiled heat exchangers, *Chem. Eng. Res. Des.* 86 (3) (2008) 221–232, <http://dx.doi.org/10.1016/j.cherd.2007.10.021>.
- [28] J. Feng, J. Fu, Z. Lin, C. Shang, B. Li, A review of the design methods of complex topology structures for 3D printing, in: *Visual Computing for Industry, Biomedicine, and Art*, Vol. 1, No. 1, 2018, <http://dx.doi.org/10.1186/s42492-018-0004-3>, Cited by: 57.
- [29] O. Al-Ketan, R.K.A. Al-Rub, MSLattice: A free software for generating uniform and graded lattices based on triply periodic minimal surfaces, *Mater. Des. Process. Commun.* 3 (2021) <http://dx.doi.org/10.1002/mdp2.205>.
- [30] I. ANSYS, ANSYS CFX-solver theory guide, 2009, Release 12.1. <https://www.ansys.com/products/fluids/ansys-cfx>.
- [31] C. Schneider, W. Rasband, Eliceiri, NIH Image to ImageJ: 25 years of image analysis, *Nature Methods* 9 (2012) 671–675, <http://dx.doi.org/10.1038/nmeth.2089>.
- [32] Q.M. Nguyen, D. Huang, E. Zauderer, G. Romanelli, C.L. Meyer, L. Ristorph, Tesla’s fluidic diode and the electronic-hydraulic analogy, *Amer. J. Phys.* 89 (4) (2021) 393–402, <http://dx.doi.org/10.1119/10.0003395>.
- [33] C. Geankoplis, Transport processes and separation, in: *Process Principles*, Prentice Hall NJ, 2003.
- [34] J. Holman, *Heat Transfer*, tenth ed., McGraw-Hill, New York, 2009.